13531/S1/1,S1/10(999-SFH)

HYDROFOIL RESEARCH PROJECT

FOR

OFFICE OF NAVAL RESEARCH

NAVY DEPARTMENT

WASHINGTON, D. C.

CONTRACT NO NONR - 507(00)

TECHNICAL REPORT NO. 8

INCEPTION OF CAVITATION ON HYDROFOIL SYSTEMS

BATH IRON WORKS CORPORATION
BY GIBBS & COX, INC.
NEW YORK 6, N.Y.

AUGUST 1952

[redacted]

ORIGINAL DISTRIBUTION LIST

Chief of Naval Research
Department of the Navy
Washington 25, D. C.
1 Attn: Code 429
4 Code 438
1 Code 466

Director
Office of Naval Research
Branch Office
150 Causeway Street
Boston 10, Mass.

Director
Office of Naval Research
Branch Office
346 Broadway
New York 13, N. Y.

Director
Office of Naval Research
Branch Office
844 North Rush Street
Chicago, 11, Illinois

Director
Office of Naval Research
Branch Office
1000 Geary Street
San Francisco 9, California

Director
Office of Naval Research
Branch Office
1030 East Green Street
Pasadena 1, California

Officer in Charge
Office of Naval Research
Navy #100, Fleet Post Office
New York, N. Y.

Supervisor of Shipbuilding and
Naval Inspector of Ordnance
85 Liberty Street
New York 6, N. Y.

Chief, Bureau of Ships
Department of the Navy
Washington 25, D. C.

Chief, Bureau of Ships
Department of the Navy
Washington 25, D. C.
2 Attn: Code 410
1 Code 518
1 Code 900

Chief, Bureau of Aeronautics
Department of the Navy
Washington 25, D. C.
1 Attn: Design Elements Division
1 Research Division

Chief, Bureau of Ordnance
Department of the Navy
Washington 25, D. C.

Chief, Bureau of Ordnance
Department of the Navy
Washington 25, D. C.
1 Attn: Assistant Chief Research
& Development Division

Chief of Naval Operations
Department of the Navy
Washington 25, D. C.
1 Attn: OP 31
1 OP 312
1 OP 312F2
1 OP 374
1 Ship Characteristics
Board

[redacted]

Commanding Officer and Director
David W. Taylor Model Basin
Department of the Navy
Washington 25, D. C.
1 Attn: Code 520
1 Code 540
1 Technical Library

Director
Naval Research Laboratory
Washington 20, D. C.
9 Attn: Code 2021

Dr. S. D. Cornell, Director
Planning Division
Research and Development Board
The Pentagon, Room 3E1036
Washington 25, D. C.

Dr. Ellis A. Johnson, Director
Operations Research Office
Department of the Army
6410 Connecticut Avenue
Chevy Chase, Maryland

Director
Weapons System Evaluation Group
Office of Secretary of Defense
The Pentagon, Room 2E995
Washington 25, D. C.

Commandant of the Marine Corps
U. S. Marine Corps
Washington 25, D. C.
Attn: G-3

Commandant
Marine Corps Schools
Quantice, Virginia
1 Attn: Marine Corps Development Center
1 Joint Landing Force Board

John S. Coleman, Secretary
Undersea Warfare Committee
National Research Council
2101 Constitution Avenue
Washington 25, D. C.

VADM E. L. Cochrane, USN (Ret.)
Maritime Administration
Washington 25, D. C.

Director of Aeronautical Research
National Advisory Committee for Aeronautics
1724 F Street, N. W.
Washington 25, D. C.

Director, Langley Aeronautical Laboratory
National Advisory Committee for Aeronautics
Langley Air Force Base, Virginia
1 Attn: Mr. F. L. Thompson

Director, Langley Aeronautical Laboratory
National Advisory Committee for Aeronautics
Langley Air Force Base, Virginia

The Hydrofoil Corporation
89-A West Street (P.O. Box 861)
Annapolis, Maryland
Attn: Mr. Paul Scherer

John H. Carl & Sons, Inc.
150 Merrick Road
Rockville Centre, New York
Attn: Mr. W. P. Carl, Jr.

Mr. J. G. Baker
Baker Manufacturing Company
Evansville, Wisconsin

Brig. Gen. F. S. Besson, Jr.
Asst. Chief of Transportation
for Operations
Room 1840, Bldg. T-7
Gravelly Point
Washington 25, D. C.

Commanding General
Department of the Air Force
Washington 25, D. C.
2 Attn: Director of Research
and Development

Dr. K. S. M. Davidson, Director
Experimental Towing Tank
Stevens Institute of Technology
Hoboken, New Jersey

Dr. L. G. Straub, Director
St. Anthony Falls Laboratory
University of Minnesota
Minneapolis, Minnesota

Reed Research, Inc.
1048 Potomac Street, N. W.
Washington 7, D. C.
Attn: Mr. Stanley Reed

Professor H. A. Schade
Department of Engineering
University of California
Berkeley 4, California

Electric Boat Division
General Dynamics Corporation
Groton, Connecticut
Attn: RADM McKee, USN (Ret.)

Bath Iron Works Corporation
Bath, Maine
2 Attn: Mr. G. B. Connard

Dr. Vannevar Bush, President
Carnegie Institution of Washington
1530 P Street, N. W.
Washington 5, D. C.

Capt. Walter S. Diehl, USN (Ret.)
4501 Lowell Street, N. W.
Washington 5, D. C.

Mr. E. G. Stout
Hydrodynamics Research Laboratory
Consolidated-Vultee Aircraft Corp.
San Diego, California

Edo Corporation
College Point
Long Island, New York
Attn: Mr. W. R. Ryan

The Glenn L. Martin Company
Middle River
Baltimore 3, Maryland
Attn: Mr. J. I. Pierson

Aerojet Engineering Corp.
Azusa, California
Attn: Mr. C. A. Gongwer

Propulsion Research Corporation
309 E. Regent Street
Inglewood, California
Attn: Mr. E. L. Hunsaker

Miami Shipbuilding Corporation
615 S. W. Second Avenue
Miami, Florida
Attn: Mr. Jean E. Buhler

[redacted]

TABLE OF CONTENTS

[redacted]

[redacted]

TABLE OF FIGURES

[redacted]

[redacted]

INCEPTION OF CAVITATION ON HYDROFOIL SYSTEMS

BY

S. F. HOERNER

ABSTRACT

This report is concerned with the inception of cavitation in flows about bodies pertinent to hydrofoil systems, for the purpose of determining the influence of various parameters and to form the background for investigations within the cavitation range. The basic phenomenon of cavitation is first discussed with respect to the influence of air content, time of exposure to low pressures, and separated flows. Minimum pressures on airfoils are related to the thickness and lift coefficient; empirical relations involving these parameters are determined which are applicable to a large class of hydrofoil shapes. The use of critical Mach numbers in determining inception values of the cavitation index, particularly for interference flows, is discussed. Cavitation data for several forms of blunt bodies are given. Considering surface roughness elements as blunt bodies, an approximate method of predicting the inception of cavitation on roughness elements in a boundary-layer flow is presented. An empirical formula is derived for the critical speed of hydrofoils and broad conclusions deduced from this study are stated.

[redacted]

INTRODUCTION

The phenomenon of cavitation, characteristic of water flows above certain critical speeds, depends upon shape and position (lift) of the considered body. Exceeding the critical speeds, the hydrodynamic characteristics of hydrofoils and other submerged components change, that is, they deteriorate. Hence, cavitation haa an important influence upon the design of hydrofoil craft, and the speeds at which cavities are first produced in the flow about hydrodynamic bodies may be looked upon as critical ones. Furthermore as the speed is sufficiently increased beyond the critical speed of inception, serious erosive effects are associated with a certain type of cavitation, An engineering study of cavitation should therefore consider a) the inception, that is the critical speed, b) the changes of the hydrodynamic characteristics, due to cavitation, and c) the phenomenon of erosion associated with cavitation. Only the first of these items will be treated in this report,, Critical cavitation numbers will be evaluated from theoretical and experimental information as found in the literature,

ITATION PHENOMENON

Cavitation comprises the phenomenon of vapor- and/or air-filled cavities within the pattern of water flows, The predominant parameter governing the onset of cavitation is the local static pressure; water tends to change from the liquid to the vapor phase wherever this pressure decreases below the vapor pressure. The vapor pressure is a function of temperature, as plotted in Figure 1 for fresh water, Sea water (with a salt content in the order of 3.2%) has a vapor pressure which is approximately 2% lower than that of fresh water, Expressed in feet of sea water (which is 2.7% heavier than fresh water) the vapor pressure of such water is consequently between 4 and 5% lower than indicated in Figure 1.

As explained in Reference 1, a necessary or helpful condition for the formation of macroscopic cavities is the presence of microscopic nuclei (air bubbles suspended in the water or clinging to solid surfaces). Consequently, "pure" water does not easily boil or vaporize; and the tendency of water to cavitate depends upon the air content, that is, upon the amount of air dissolved and/or suspended in the water, The tendency has been tested in transparent nozzles, such as illustrated in Figure 2, Because of the contraction of the cross-sectional area, the static pressure of the water flowing through these nozzles decreases, and visible cavitation (formation of bubbles) is produced under proper conditions. Figure 3 shows the pressure measured at the inception of cavitation in fresh water, as

obtained in tests at the David Taylor Model Basin (References 2 and 3) in which the relative air content was varied, This pressure (which may be termed critical pressure) is seen to decrease with the air content. For small air content, considerably negative pressures are necessary *to* start cavitation and vaporization, meaning that tensions exists within the water.

Time is another physical parameter affecting the inception of cavitation, Consider a volume of water passing through a bow pressure field; the time during which this volume is exposed to the cavitation-causing pressure is

$$\text{time} \propto \frac{\text{length of pressure field}}{\text{velocity}} \propto \frac{\text{body dimension}}{\text{velocity}} \qquad (1)$$

A change from the liquid to the vapor phase requires a certain time. Consequently, the critical. cavitation number of the hemispherical head, illustrated in Figure 4, increases with the time as defined by Equation 1.

Summing up, the vapor pressure presents only an approximate condition for the onset of cavitation; yet this pressure is generally considered the most important parameter indicating favorable conditions heading to cavitation, The "preparedness" of a water flow in respect to cavitation is indicated by the cavitation number

$$\sigma = \frac{P_{amb} - P_{vapor}}{q} \qquad (2)$$

where p_{amb} is the "ambient", that is the static pressure within the undisturbed flow and $q = 0.5 \rho V^2$ is the dynamic pressure of the flow. The smaller the cavitation number, the stronger is the tendency of a water flow to cavitate.

The cavitation number at which cavities first form in the flow about a body is called the critical cavitation number σ_i. The onset of cavitation may be determined in several ways, viz., by visual observation of the first appearance of cavitation bubbles, by the sharp increase in sound level of the flow when these bubbles collapse, or by the divergence of drag, lift or moment coefficients from their undisturbed values; usually the drag increases and the lift decreases upon exceeding the critical speed, because of a change of the flow pattern. The critical number depends upon shape and attitude of the considered body, that is, upon the pressure distribution (usually upon the minimum of this distribution). "Theoretical" critical numbers can, therefore, be derived from the published pressure-distribution material on aerodynamic bodies. Cavitation may be expected to occur if

$$\sigma \leq \sigma_i = -\left(\frac{\Delta p}{q}\right)_{min} \qquad (3)$$

where $\Delta p_{min} = p_{min} - p_{amb}$ corresponds to the measured (or calculated) pressure minimum around a body immersed in a flow of water (or incompressible air).

The Numachi-type nozzle, illustrated in Figure 2, shows

cavitation at pressures (measured on the nozzle wall) which are considerably higher than those in the continuous Venturi nozzle. According to observations, cavitation first begins within the cores of the vortices associated with the separation behind the narrowest section of the Numachi nozzle. Evidently, the pressure within these vortex cores is appreciably lower than the minimum on the nozzle wall, A corresponding result is reported in Reference 4, where the blunt head of a three-dimensional body, with a separated flow pattern, shows a critical cavitation number which is more than twice as high as the minimum static pressure coefficient (Equation 3) measured at the surface of the body (Figure 2B) shortly before the onset of cavitation,

[redacted]

DEPENDENCE OF [C CAVITAT[ON NUMBER UPON NESS

Considering symmetrical foil (or strut) sections at zero lift, the magnitude of the minimum pressure coefficient depends upon the distribution of thickness along the chord. For instance, elliptical sections, which have a location of the maximum thickness at $X = 0.5\,c$, have theoretically (neglecting the second-order term)

$$\frac{p_{min} - p_{amb}}{q} = \left(\frac{\Delta p}{q}\right)_{min} = -2\,\frac{t}{c} \qquad (4)$$

which actually holds up to, and possibly above, $t/c = 0.40$. Figure 11.16 of Reference 5 indicates an approximate method of determining $(\Delta p/q)_{min}$ when the location of the maximum thickness is forward of mid-chord, by considering the effective thickness ratio $t/(2x)$ Instead of t/c. Sections with $t/(2x)$ = constant, are expected to have approximately the same maximum velocity ratio, independent of the length of the portion $(c - x)$, behind the maximum thickness. Figure 5 shows the maximum negative-pressure coefficients of various types of symmetrical foil sections (at zero lift) plotted against $t/(2x)$ adequately represented by

$$\left(\frac{\Delta p}{q}\right)_{min} = 2.1\,\frac{t}{2x} \qquad (5)$$

This evaluation proves to be consistent at Peynolds numbers above the critical (in respect to flow separation at the rear), up to locations $X = 0.5\,c$, and up to effective thickness ratioa in the order of 0.40.

The NACA 64- and 65-Series foil sections (Reference 6) have been developed so that the pressure continues to decrease as far back as possible in order to preserve laminar boundary-layer flow. It is found that the minimum pressure coefficients for these sections do not "collapse" to the same function of $t/(2x)$ as the other families do. These sections are not favorable in respect to avoiding the onset of cavitation, at or in the vicinity of zero lift.

According to Equation 3, critical cavitation numbers are expected to coincide with the minimum pressure coefficients in Figure 5. However, the available cavitation tests (Reference 7, for instance) show such a scatter (at zero lift) above and below the expected line, that they cannot be considered proof or disproof of the correlation between cavitation number and pressure distribution.

INFLUENCE OF LIFT ON THE CRITICAL NUMBER

The static pressure *is* further **reduced** on the **upper** or suction side upon setting a foil section at an angle of attack to produce lift, Theoretically, for low lift coefficients, the average additional **pressure** differential due to lift **is**

$$\left(\frac{\Delta p}{q}\right)_L = -0.5 C_L \qquad (6)$$

The lift, **is, however,** not **uniformly** distributed over **the** chord; the pressure **minimum** *is* accordingly higher than the average. **The** pressure **distribution** and the minimum **due** to lift depend **upon** the shape of the camber line.

Cambered sections have an "optimum" **lift** coefficient, that is, a condition **where the** streamlines meet the **section nose** without **flowing around** from one **side** to the other. Single-arc sections, for instance, **with a flat** lower side, have an **optimum angle** of attack (measured **against** the **lower side** and in two-dimensional flow) **equal** to **zerc; their** optimum **lift.** coefficient **is approximately**

$$C_{L_{opt}} = 6(t/c) \qquad (7)$$

In **regard** *to* cavitation, **operation** in **the** vicinity of this optimum is **expected** to provide **the** highest **possible** critical **speeds** for a given foil section at **the respective** lift **coefficient, Available test data** presenting **the minimum** pressure coefficients of **foil** sections at or near the optimum

lift coefficient, nave been plotted in Figure 6. The two pressure contributions, one due to thickness (at $C_L = 0$) and another due to lift, appear superimposed, Subtracting the thickness component (as presented in Equation 5) the lift component is found to be approximately independent of the thickness ratio for certain families of sections. According to Figure 7,

$$\left(\frac{\Delta p}{q}\right)_{min\,L} = -k\,C_L \qquad (8)$$

The magnitude of the constant k depends upon the absolute and relative location of thickness and camber. The lift is predominantly located in the forepart of a foil section, with the center usually between 25 and 30%of the chord. Combining, for example, such a pressure distribution with that due to a thickness location at 50% of the chord, a value of $k = 0.7$ is found in Figure 7. On the other hand, superimposing to the lift distribution, the pressure minimum caused by a location of the maximum thickness in tne vicinity of 30% of the chord, a noticeably higher factor is found, $k = 0.65$, for sections such as NACA 2412, for instance, or M-12, or many of the old Goettingen sections (Reference 8).

Figure 6 shows one set of experimental pressure coefficients representing the NACA 64- and 65-Series sections. Combining these results with a theoretical point at $C_L = 0$, a non-linear function $(\Delta p/q)_L = f(C_L)$ is obtained, with favorable pressure conditions between $C_L = 0.3$ and 0.5. Within this range, the contribution due to thickness of these sections, evidently combines favorably with that due to lift, presenting

a botal pressure coefficient which is fairly low (but not lower than that of circular-arc aections).

Three sets of actual cavitation tests are included in Figure 7. Two of these results (with σ_{i_L} defined by the divergence of drag and/or lift coefficients) agree well with the respective two branches as predicted from the pressure analysis. The Aerodynamische Versuchsanstalt (AVA) results on a systematic aeries of marine propeller eectiona (according to Reference 9), with maximum thickness location at 50% of the chord, with mostly flat lower sides and with well-rounded leading edges, indicate critical cavitation numbers (defined by the deviation of drag and lift coefficients) which are more favorable than those of comparable circular-arc sections having the usual pointed noses. The factor k is less than 0.6 for these shapes, Evidently, the rounded nose and the camber distribution help to produce a lift coefficient which is high in relation to the minimum pressure coefficient,

In cases where the flow pattern around the foil nose is not "optimum" (that is, with flow from the lower to the upper side), super-velocities and pressure differentials must eventually be expected which are higher than those given by Equation 8. In this respect, Figure 8 presenta the critical cavitation number of a series of symmetrical sections with $t/c = 13.33\%$, depending upon the lift coefficient. Surprisingly, the shape of these sections, varying between a pointed and a rounded nose,

and between 35 and 50% thickness location, does not noticeably or consistently change the critical cavitation number.

Upon increasing the lift above the optimum coefficient, an additional and narrow negative pressure peak originates on the auction aide, near the leading edge. This peak grows and exceeds the value indicated by Equation 8, at a lift coefficient which (for average wing sections) is between 0.1 and 0.2 higher than the optimum coefficient, Above such lift cobfficienta, the critical cavitation number might, therefore, be expected to correspond to the additional pressure peak, Such peak coefficients are plotted in Figure 8 for 12 and 15% thick symmetrical sections (from Reference 10) having roughly the same nose shape as the rounded 13.3% sections of Reference 7. The cavitation tests on the latter ones show visual inception of cavitation (and force divergence closely following visual inception) at cavitation numbers which are much lower (roughly half as high) than the values of the nose–pressure coefficients, A possible explanation is that the oncoming (laminar and fully attached) flow does not have time to develop a steady-state cavity upon passing through the narrow region of the pressure peak as previously explained, Assuming that the chordwise extension of the peak is 3 per cent of the 8 inch chord, the time during which the water particles were exposed to pressures below the critical is in the order of 2/10,000 of a second, for an average critical speed of 25 knots as observed in Reference 7.

[redacted]

Assuming that some little cavitation may develop above the nose in the case of Figure 8, this evidently disappears aft of the pressure peak without unfavorably affecting the flow pattern. Indeed, there is evidence that at angles of attack higher than "optimum", the lift coefficient of a section may increase (at constant angle of attack under otherwise favorable conditions), upon slightly exceeding the critical cavitation speed (Reference 9). Thus, sharp, negative peaks in the pressure distribution cannot necessarily be considered being responsible for the onset of cavitation or the subaequent changes in the flow pattern; the length (chordwise extension) of a low-pressure field seems to have appreciable influence upon the inception of cavitation. Another indication of this fact is evident in Figure 8 of Reference 11. Good agreement between σ_i and $(\Delta p/q)_{min}$ is found there within 6° of the angle-of-attack range; however, outside *of* this range, σ_i is considerably lower than the pressure coefficients which were measured in wind tunnel teats,

No further specific information on the correlation between pressure peaks and cavitation seems to be available at the present time. There ia, however, an analogy in the field of compressible aerodynamics. The critical Mach number of sharp-nosed sections at lift coefficients different from their optimum does not correspond to the maximum super-velocity around their leading edges; a delay of the *drag* and lift divergence by $\Delta M = 01$ to 02, or even higher, beyond the theoretical Mach number, has been found in experiments (see Figure 11.21 of Reference 5 or Figure 169 of Reference 6).

[redacted]

CAVITATION NUMBER AS A FUNCTION OF MACH NUMBER

In compressible aerodynamics, the theoretical critical Mach number (indicating the first appearance of local velocities equal to that of sound) is a function of the minimum pressure coefficient in incompressible flow (at low speeds). It has been mentioned in the preceding section that neither cavitation nor critical Mach number effects respond to sharp pressure peaks. Confining, however, the analysis to flow patterns where no such peaks are involved, it is possible to predict critical cavitation numbers on the basis of critical Mach numbers M_{cr} known from wind-tunnel tests using the theoretical function $(\Delta p/q)_{min}$ versus M_{cr} as plotted on Page 114 or in Figure 149, respectively, of Reference 6. For three-dimensional flow patterns, this function seems to be approximately the same as for two-dimensional sections.

Evaluating, for example, Figure 11.12 of Reference 5, the critical Mach number of a wing cross (the crosswise junction of two foils) at zero lift is found to be approximately 0.67, as compared to 0.74 for the employed 12% thick foil section. The corresponding prediction for the critical cavitation number is $\sigma_i = 0.62$ for the foil junction as compared to 0.34 for the section. In a similar case (Reference 12), the critical Mach number of a 12% thick foil section is reduced from 0.78 to 0.71 upon adding a 10% thick fin. The corresponding critical cavitation numbers are $\sigma_i = 0.28$ and 0.48, respectively.

According to Figure 11.26 of Reference 5, a fuselage in symmetrical flow at zero lift does not affect the critical Mach number of a swept *wing*. Engine nacelles, however, reduce the critical Mach number from 0.81 to 0.75, which would mean an increase of the critical cavitation number from 0.23 to 0.36, at zero lift for that particular configuration. Similar predictions can be derived for other combinations of wings, bodies and/or appendages for which wind-tunnel test results giving the critical Mach number am available.

Generally, the mentioned interference effects are concentrated at the junctures between foils or bodies with struts, nacelles, or appendages. The effect of cavitation at the junctures upon the total resistance of a foil system may, therefore, be quite small; the more important issue in such cases may be the local erosion caused by cavitation.

The influence of the aspect ratio (Figure 11.19 of Reference 5) or that of the angle of sweep (Figure 11.25 of Reference 5) upon the critical cavitation number can also be predicted on the basis of the critical Mach number, if the latter one is known as a function of these parameters. To facilitate such estimates, the standard speed as defined by Equation 17 was plotted in Figure 9 against the critical Mach number. However, to show the limitations of the method, the facts concerning the sphere (at supercritical Reynolds numbers) shall be listed here. According to Figure 11.5 of Reference 5, the critical Mach number (at which the drag

coefficient diverges from the value at lower Mach numbers) is $M_{cr} = 0.68$. The pressure coefficient which corresponds to this Mach number according to the principle as outlined above, is found to be $(\Delta p/q)_{min} = -0.57$. Actually, however, this value is known to be in the order of - 1.1 for the flow pattern at supercritical Reynolds numbers. From experience with other bodies, it is believed that the compressible flow pattern favorably combines with the boundary layer flow, thus delaying the divergence of the *drag* coefficient beyond the Mach number at which the speed of sound is first attained on the surface of the considered sphere. Such an interaction is likely to occur on rounded bodies with more or less separated flow pattern.

CRITICAL CAVITATION NUMBERS OF BLUNT BODIES

The term "blunt" is applied here to all types of bodies which are not slander and "streamlined"; such as spheres, circular cylinders or square bodies.

Circular Cylinder

The flow pattern of the circular cylinder (in cross flow) changes within a critical range of the Reynolds number R_d = (1 to 4) 10^5. Below this range, the flow is eeparated from the rear of the cylinder. Due to this separation and the vortex system resulting from it, the critical cavitation number is higher, σ_i = 1.9 (according to Reference 13) than the minimum pressure coefficient, $(\Delta p/q)_{min}$ = - 1.6. On the other hand, above the critical Reynolds number, the flow pattern shows a higher value of the minimum pressure coefficient, $(\Delta p/q)_{min} \approx$ - 2.0. The cavitation number at which the drag coefficient diverges, seems to vary between σ_i = 1.8 (which means a delay of the onset, Reference 13) and σ_i = 2.4 (Reference 14). Again, the boundary lager may be responsible for this difference by *way* of an interaction with cavitation.

Ellipsoidal Bodies

Basically, three-dimensional bodies show supervelocity ratios which are lower than those around two-dimensional ones (considering equal thickness ratios), At the sides of ellipsoidal bodies, the supervelocity

ratio is approximately

$$\left(\frac{\Delta V}{V}\right)_{max} = 0.6\left(\frac{d}{L}\right)^{3/2} \tag{9}$$

The corresponding critical cavitation number fa expected to be

$$\sigma_i \approx -\left(\frac{\Delta p}{q}\right)_{min} \approx 1.2\left(\frac{d}{L}\right)^{3/2} \tag{10}$$

According to Figure 10, this equation holds approximately true, down to $L/d = 1$ (a sphere), Pressure-distribution tests (Reference 15) on a series of streamlined bodies with maximum thickness at 40% of the length, indicate a constant in the order of 1.6 (instead of 1.2) owing to the thickness location different from mid-length,

Employing half of an ellipsoidal *body* as head of a cylinder (in axial flow), the supervelocities *are* reduced because of the presence of such a cylindrical afterbody. As shown in Figure 10, tests of various head forms (Reference 4) show correlation between the critical cavitation number and the minimum pressure coefficient; cavitation started, however, during these tests (in the form of visual bubblea at the position of minimum pressure) at σ values which are roughly 15% higher than the corresponding pressure coefficients.

Wear $(2x)/d = 0$, in Figure 10, there is again a larger difference between the values of σ_i and $(\Delta p/q)_{min}$, this time in the order of

3 to 1, associated with a aeparated flow pattern (formation of vortices). The values within the region between here and $(2x)/d = 1$ are expected to depend upon Reynolds number and boundary-layer conditions of such bodies.

Surface Roughness

No data on the influence of roughness on the inception of cavitation appear to exist in this country, In the absence of experimental evidence, one may construct an approximate analysis to obtain an idea of the influence of roughness on inception,

Roughness consisting of small bodies (grains) of, for instance, hemispherical shape, may also encounter cavitation. Considering the low Reynolds number of such roughness elements, the flow pattern must be assumed to be separated, Based upon the local (average) velocity within the boundary layer, the critical cavitation number *may*, therefore, be in the order of $\sigma_i = 1$, as taken from Figure 10. The corresponding standard local critical speed is approximately 27 knots, as found in Figure 11.

Assuming turbulent boundary-layer flow, the average or effective local velocity V_h corresponding to the height h of a roughness element, is approximately (according to Page 49 of Reference 5)

$$V_h/V = 0.86\,(h/s)^{1/6} \qquad (11)$$

valid up to $h = s$, where s = thickness of the boundary layer.

Assuming the critical speed V_h = 27 hots, it is seen that the speed of the body, required to produce cavitation, is 31 knots for $h = s$, for example. For a roughness element with h = 1% of the boundary-layer thickneaa, V_{cr} = 67 knots.

On a surface with uniform roughness distribution, cavitation is expected to start first near the leading edge (where the Boundary-layer thickness is smallest). Considering an ieolated spot of roughness at distance x, the thickness *may* be assumed to be between 1.5 and 2% *of* the travelled length (for average practical conditions), The thickness may also be found by combining Equations 2.18 and 2.19 of Reference 5, giving

$$s/x \approx 5\, C_{fx} \qquad (12)$$

where C_{fx} = skin-friction drag coefficient of a surface with the length x.

Since nothing seem to be known about the effect of cavitation upon the frictional drag, further analysis of the critical speed is considered to be premature.

THE CRITICAL SPEED OF HYDROFOILS

Considering boats with hydrofoils operating close to the surface of water, p_{amb} may be assumed equal to the atmospheric pressure. The aeronautical standard of this pressure is

$$p_{amb} = 2120 \text{ lbs/ft}^2 \tag{14}$$

corresponding to a head of approximately 33 feet of sea water, At a standard temperature of 59°F, the vapor pressure of fresh water is very low, in the order of 1.6% of the atmospheric pressure; the corresponding heed is approximately 0.5 ft of water. Disregarding thia small quantity, the cavitation number defined by Equation 2 simply reduces to the ratio of the static pressure p_{amb} to the dynamic flow pressure $q = 0.5\rho V^2$. Thus, the critical dynamic pressure

$$q_{cr} \approx p_{amb} / \sigma_i \tag{15}$$

Sea water within the interface, usually has a high air content (practically saturated) on account of contact with the air and nave motion, Tests kith such water (Reference 2), in a continuous Venturi nozzle, show incipient cavitation (formation of presumably air-filled bubbles) at pressures corresponding to between 2 and 5 feet of water. This decrease in available pressure is compensated by the increase in pressure due to foil submergence and the net effect may be assumed to be close to zero for typical hydrofoil applications, Combining Equations 14 and 15,

$$q_{cr} \approx 2120/\sigma_L \qquad \text{(lbs/ft}^2\text{)} \tag{16}$$

Using the standard sea water density of $\rho = 1.99$ (lbs sec^2/ft^4), the corresponding "standard" critical speed of hydrofoil systems is

$$V_{cr} = 0.59\sqrt{\frac{2}{1.99}\,\frac{2120}{\sigma_L}} = \frac{27}{\sqrt{\sigma_L}} \qquad \text{(knots)} \tag{17}$$

where 0.59 accounts for the conversion of ft/sec to knots. Figure 11 presents a plot for this function. Corrections for submergence or air content, and for temperatures or pressures different from the atmospheric standard, can be applied to Equation 16.

Under the standard conditions defined in the preceding paragraph, it is possible to predict so-called standard critical speeds for given shapes and angles of attack. For example, combining Equations 5 and 8 with Equation 17, the critical speed of a hydrofoil section is found to be

$$V_{cr} = \frac{27}{\sqrt{2\frac{t}{(2x)} + 0.7\,C_L}} \qquad \text{(knots)} \tag{18}$$

with rounded-off constants of 2 and 0.7. This function is plotted in Figure 12 for three thickness ratios.

SUMMARY AND CONCLUSIONS

a) Although the inception of cavitation depends upon secondary parameters such as air content and time (size), the cavitation number is still employed to indicate the tendency of a water flow to cavitate on a body.

b) In many cases the critical cavitation number is closely related to the minimum pressure coefficient prevailing on the surface of a body. However, thie correspondence does not hold in cases of separated patterns (vortex flows) and for flows with narrow pressure peaks.

c) The critical cavitation number and the corresponding critical speed of hydrofoil sections is derived as a function of thickness ratio and lift coefficient. Favorable sections can be found on the basis of this analysis.

d) Both the critical cavitation number and the critical Mach number are functions of the minimum pressure coefficient on the surface of a considered body. Under certain conditions, the inception of cavitation can, therefore, be predicted if the critical Mach number is known from experiment.

e) Blunt bodies have comparatively high critical. cavitation numbers, on account of high supervelocity ratios and/or because of flow separation (vortex pattern).

f) A tentative prediction is presented in regards to the critical cavitation speed of rough surfaces.

g) This report deals only with the critical cavitation number or speed, Further studies should be made considering the changes of drag and lift coefficients due to cavitation and the conditions of erosion.

REFERENCES

1) Eisenberg; On the Mechanism and Prevention of Cavitation, Navy TMB Rpt No. 712 (1950).

2) Crump; Critical Pressures for the Inception of Cavitation in Fresh and Sea Water as Influenced by Air Content, TMB Rpt 575 (1949).

3) Crump; Critical Pressures for the Inception of Cavitation in a Numachi Nozzle as Influenced by the Air Content, TMB Rpt 770 (1951).

4) Rouse and McNown; Cavitation and Pressure Mstribution - Head Forms at Zero Angle of Yaw, Iowa State University Studies Eng. Bull. 32 (1948).

5) Hoerner; Aerodynamic Drag, 1951,

6) Abbot, von Doenhoff, Stivers; Summary of Airfoil Data, NACA Tech Rpt 824 (1945).

7) Benson, Land, Havens; Tank Testa of Ship-Propeller Strut Sections, NACA (Langley) Memo Rpt 16, April 1942 for Bureau of Ships, Navy Dept.

8) Schrenk; Pressure Distribution Along the Chord of Wing Sections, Contribution IAll in Ringbuch Luftfahrttechnik, German Ministry for Aeronautics, 1938.

9) Walchner; Contribution to the Design of slip Propellers Without Cavitation, AVA Monograph, Reports and Translations No. 330 (1947), British Ministry of Aircraft Production, See also NACA Tech Memo 1060.

10) German Rpt ZWB FB 1621 (1943); Aerodynamic Forces and Pressure Distribution on a Series of Airfoil Sections,

11) Daily; Cavitation Characteristics of a Hydrofoil action, Trans ASME 1949, p. 269.

12) Hilton, Moor, and Sargent; High-Speed Tunnel Measurements on Fin-Tailplane Interference, British ARC RM 2138 (1941).

13) Pond and Bledsoe, Pressure Distribution Tests on Modified Ellipsoidal Nose Shapes, TMB Report C-456 (1951).

14) Martyrer; Force Measurements on Cylinders and Foils at Cavitation-; in Kempf-Foerster, Hydrodynamische Problem des Schiffsantriebs, Hamburg 1932.

15) Lange; Tests on a Systematic Series of Fuselage Bodies, German Rpt ZWB FB 1516.

16) Numachi and Kurokawa; Several Papers on Inception of Cavitation as a Function of Air Content; Tech Rpts Imp. University Tokyo Vol 12 (1938) p. 422, 529, 591, 604; Werft Reederei Hafen Vol 20 (1939); Trans and Commentary, Ordn, Res. Lab. Penn State College, August 1946.

17) Parkin; Scale Effects in Cavitating Flow, California Institute of Technology (CIT) Hydrodynamics Laboratory, Dr.Thesis 1952.

18) Goethert and Richter; Tests on NACA 0 00 15 - 1,1 40 Section in the DVL High-Speed Tunnel, Jahrbuch D. Luftfahrtforschung 1941 p. I 101.

19) Fage, Falkner, Walker; Experiments on a Series of Symmetrical Joukowsky Sections, Brit. ARC RM 1241 (1929).

20) Graham, Nitzberg, Olson; Pressure Distributions at High Speeds Over Five Airfoil Sections, NACA Tech Rpt 832 (1945).

21) NACA; On the pressure Distribution of 64- and 65-Series Sections, Tech Notes 1167 (1947) and 2177 (1950).

22) Balhan; Study of Some Propeller-Blade Sections in Cavitating Flow, Dr.Thesis, published as No. 99 by Scheepsbouwkundig Proefstation, Wageningen Nethesland, 1951.

23) Holl; Investigation of Propeller-Blade Sections Having Reduced Cavitation Tendency, Forschung 1932 p. 109.

24) Gutsche; Characteristics of Propeller-Blade Sections; a) Mitteilungen Pr. Versuchsanstalt Wasserbau Schiffbau, Heft 10 (Berlin 1933), b) Yearbook Schiffbautech Gesellschaft 1936 p. 277; 1938 p. 125; and Vol. 41 (1940).

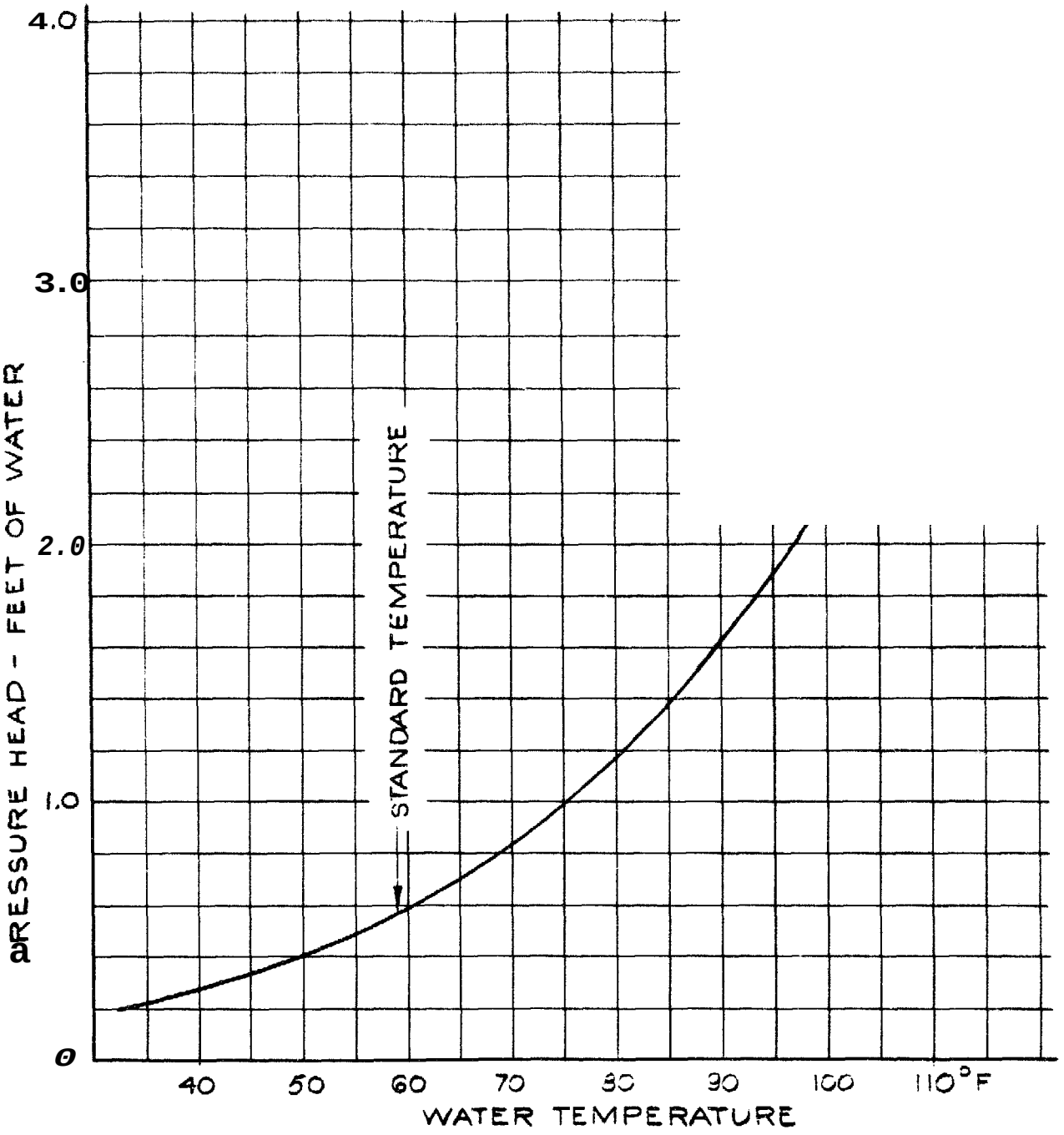

VAPOR PRESSURE OF FRESH WATER

GIBBS & COX ING. GRAPH NO. HGR 13531-2-SI-1-130 AUGUST 1952

FIGURE NO. 1

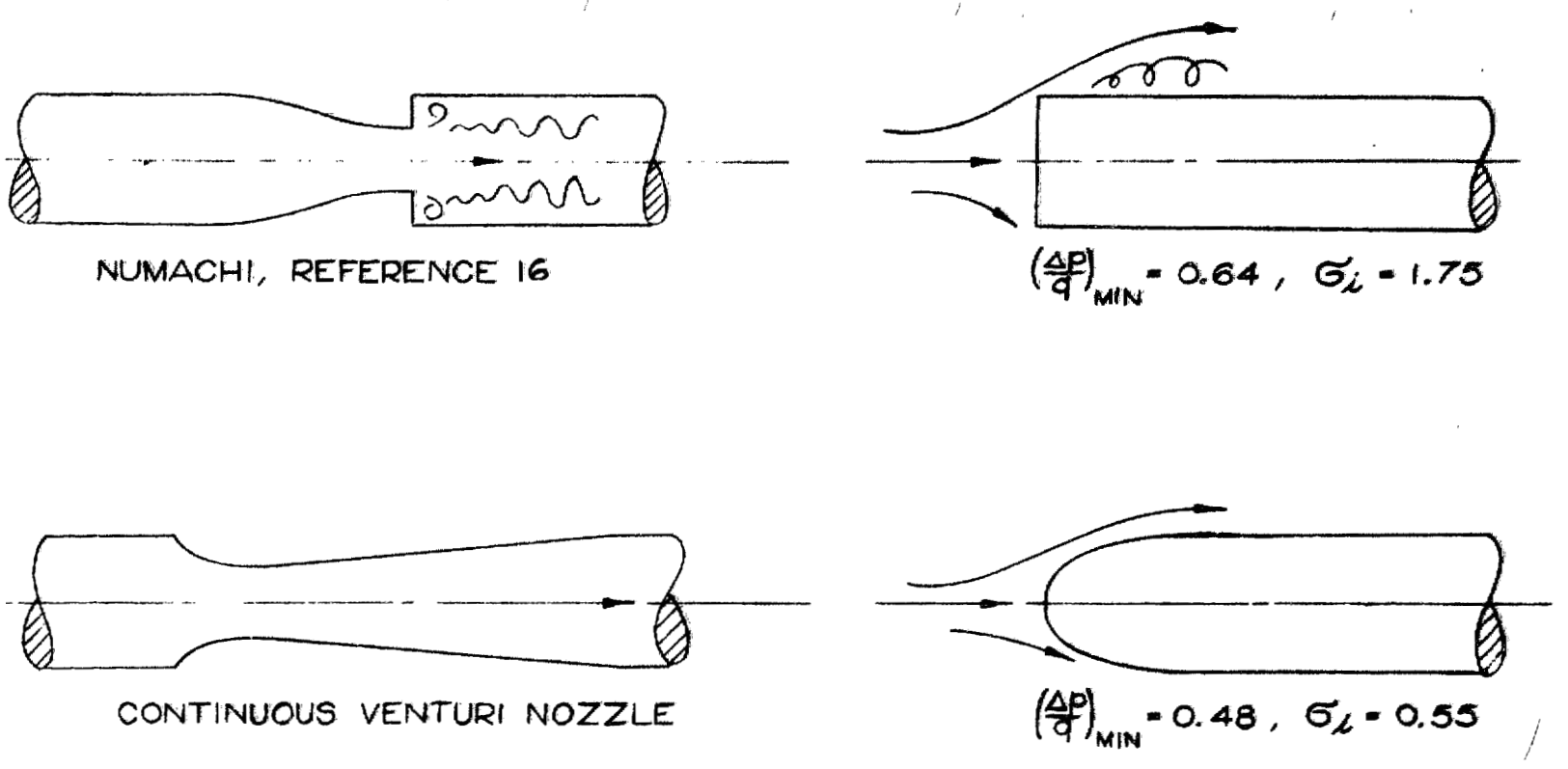

(A) SHAPE OF TEST NOZZLES (REFERENCES 2 AND 3)

(B) FLOW PATTERN PAST BLUNT BODIES (REF. 4)

INFLUENCE OF THE FLOW PATTERN UPON THE ONSET OF CAVITATION

GIBBS & COX INC. SKETCH NO. HSK 13531-2-51-3-17 JULY 1952

FIGURE NO. 2

GIBBS & COX, INC.

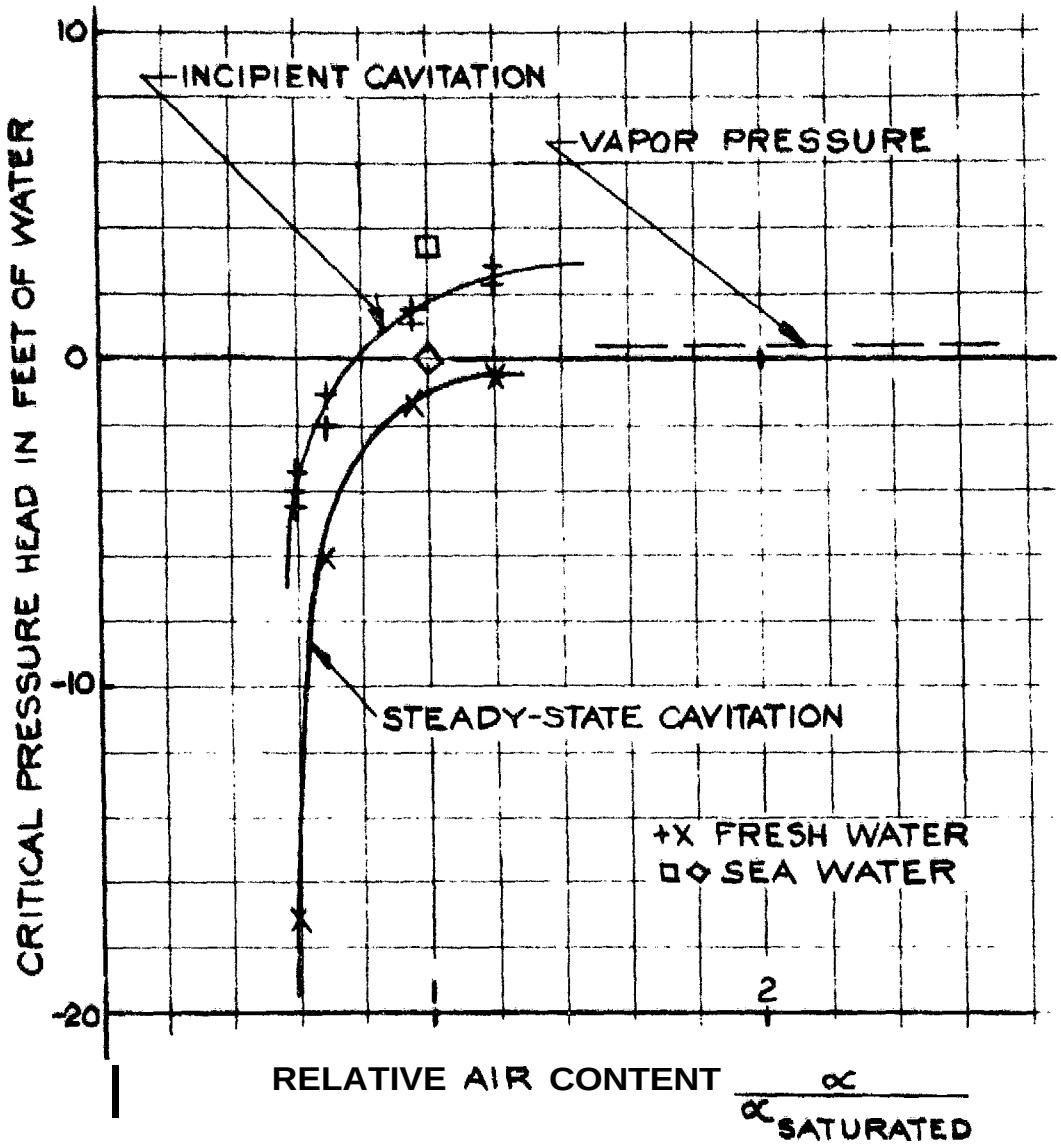

CRITICAL PRESSURE: (FOR INCIPIENT CAVITATION)
AS A FUNCTION OF RELATIVE AIR CONTENT.
OBTAINED FROM TESTS WITH A VENTURI NOZZLE.
(DATA FROM REFERENCES 1 & 2)

GIBBS & COX INC. GRAPH NO. HGR 13531-2-S1-1-135 AUGUST 1952

DATA FROM CIT EXPERIMENTS
ANALYZED IN REFERENCE 17

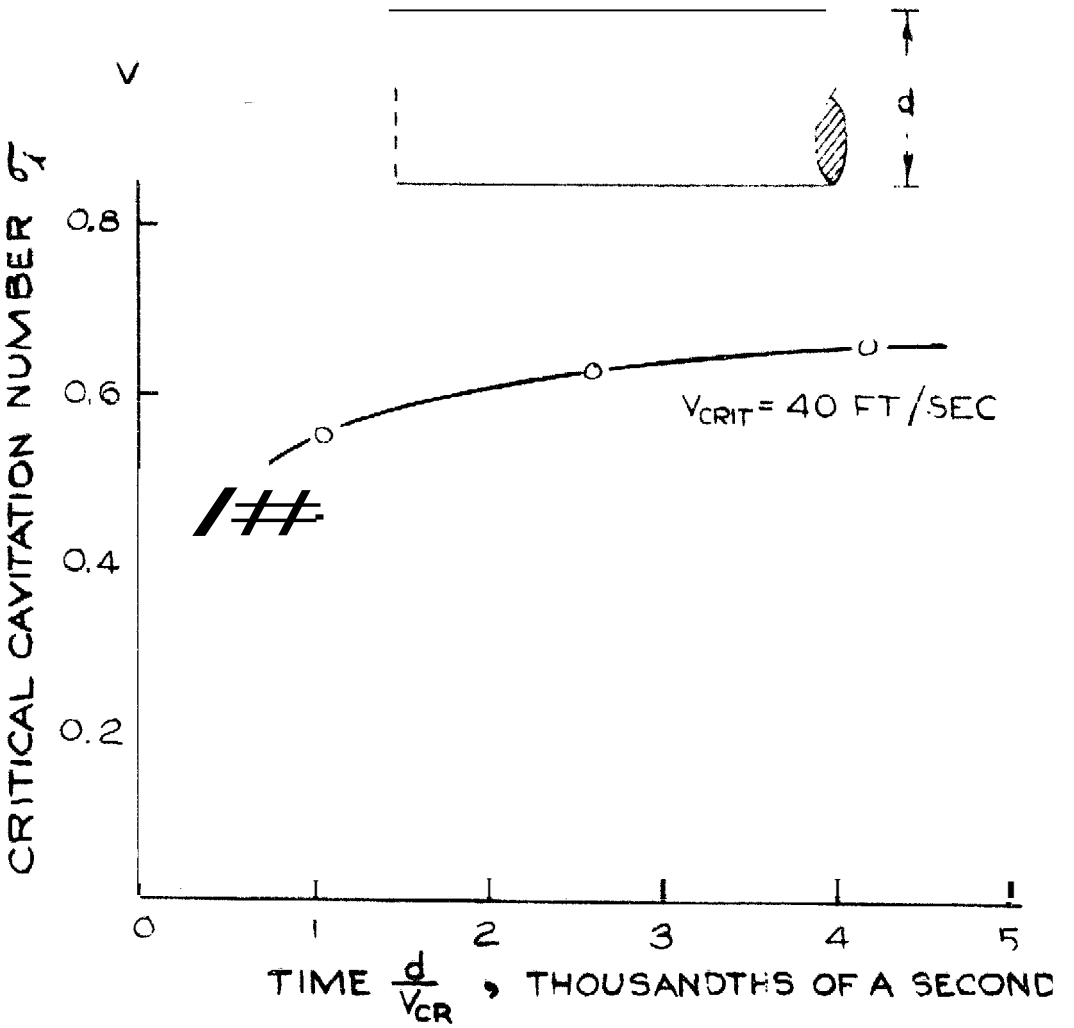

INFLUENCE OF TIME UPON THE CRITICAL CAVITATION NUMBER

GIBBS & COX INC. GRAPH NO.HGR-13531-2-SI-1-126 JULY 1952

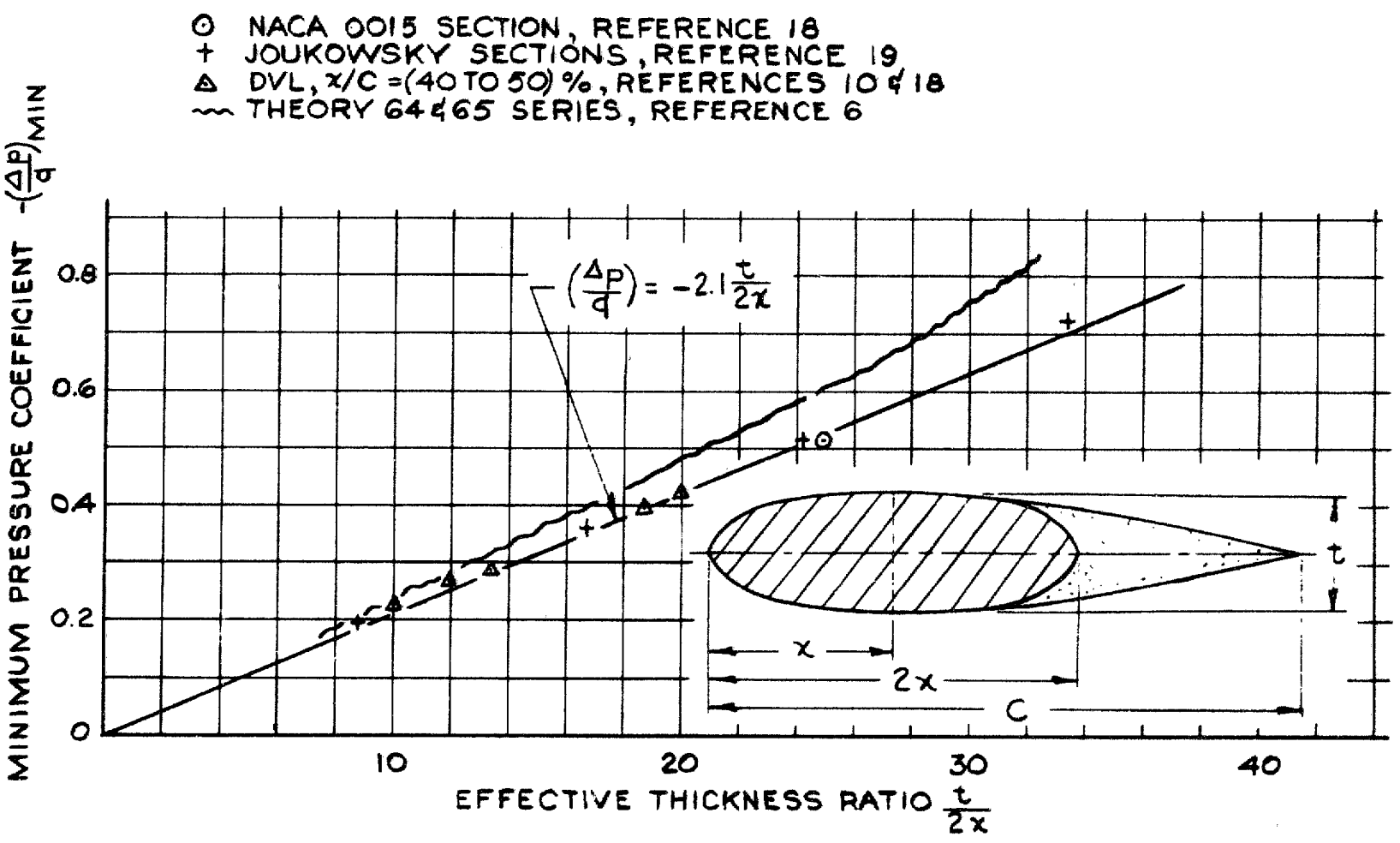

MINIMUM PRESSURE COEFFICIENT AT THE SIDES OF SYMMETRICAL SECTIONS AT ZERO ANGLE OF ATTACK

GIBBS & COX INC. GRAPH NO. HGR 13531-2-SI-1-124 JULY 1952

FIGURE NO. 5

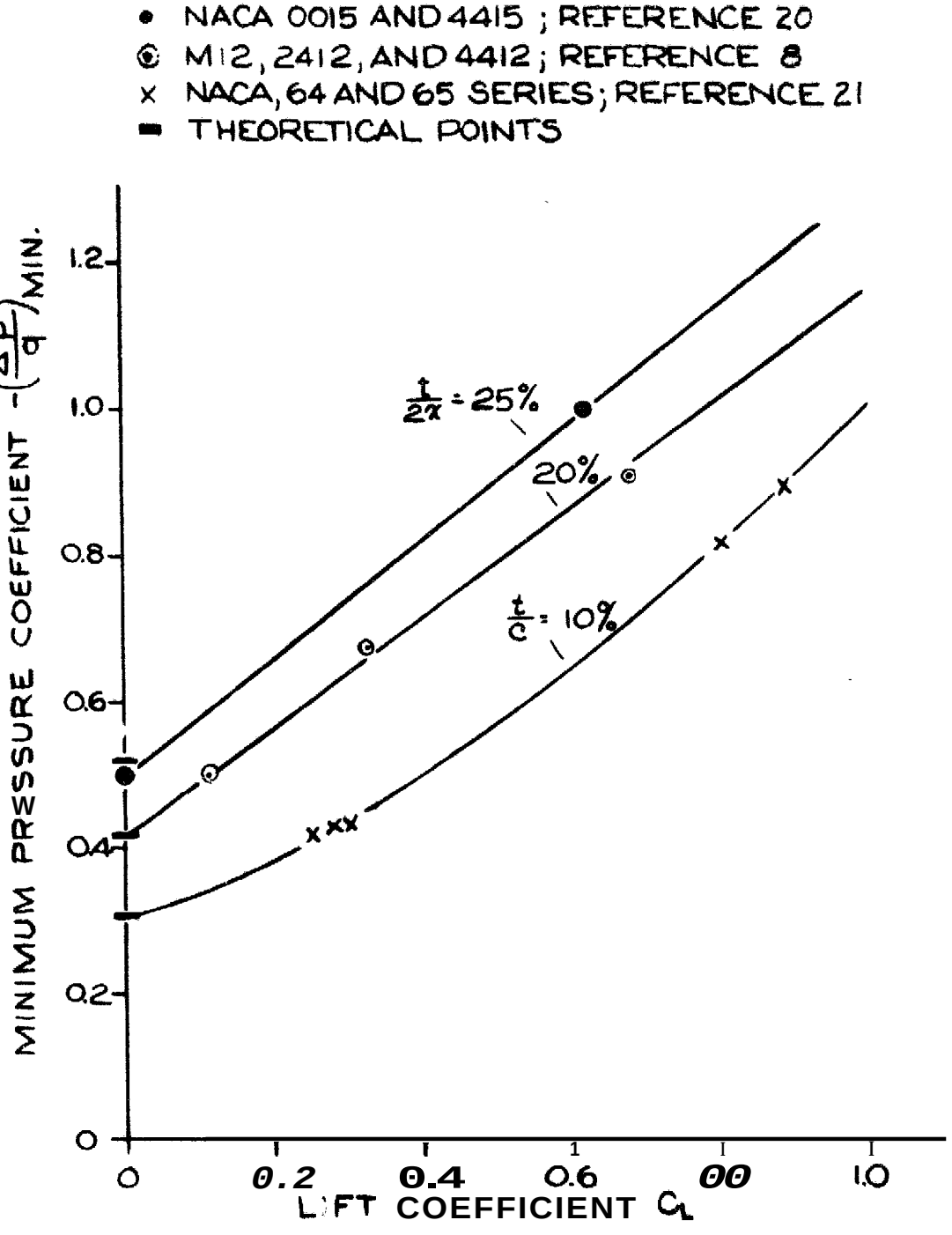

THE MINIMUM PRESSURE COEFFICIENT ON THE UPPER SIDE CAMBERED FOIL SECTIONS

GIBBS & COX INC. GRAPH NO. HGR 13531-2-SI-1-128 JULY 1952

P	○	RINGBUCH, $\chi/C \approx 30\%$, REFERENCE 8
P	+	GUTSCHE, $\chi/C = 30\%$, REFERENCE 24
C	■	MARTYRER, $\chi/C = 30\%$, REFERENCE 14
P	△	MOLL, $\chi/C = 50\%$, REFERENCE 23
P	▽	GUTSCHE, $\chi/C = 50\%$, REFERENCE 22
P	□	RINGBUCH, $\chi/C = 50\%$, REFERENCE 8
C	●	WALCHNER, $\chi/C = 50\%$, REFERENCE 9
C	*	AVA, $\chi/C = 50\%$, REFERENCE 9

P - PRESSURE DISTRIBUTION MEASUREMENTS
C - CAVITATION TESTS

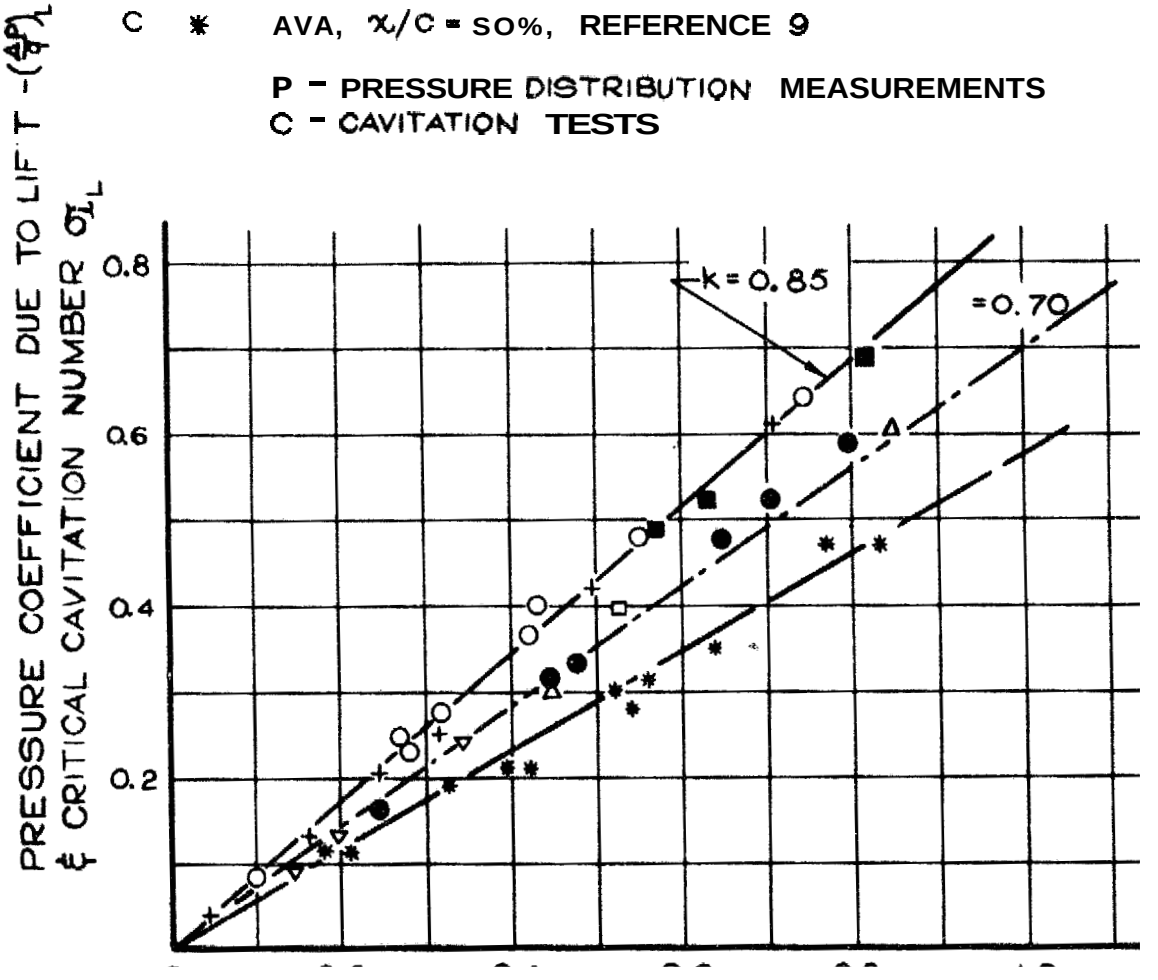

PRESSURE COEFFICIENT DUE YO LIFT
FOR VARIOUS FOIL SECTIONS
AT OPTIMUM LIFT COEFFICIENTS

GIBBS & COX INC. GRAPH NO. HGR13531-2-SI-1-127 JULY 1952

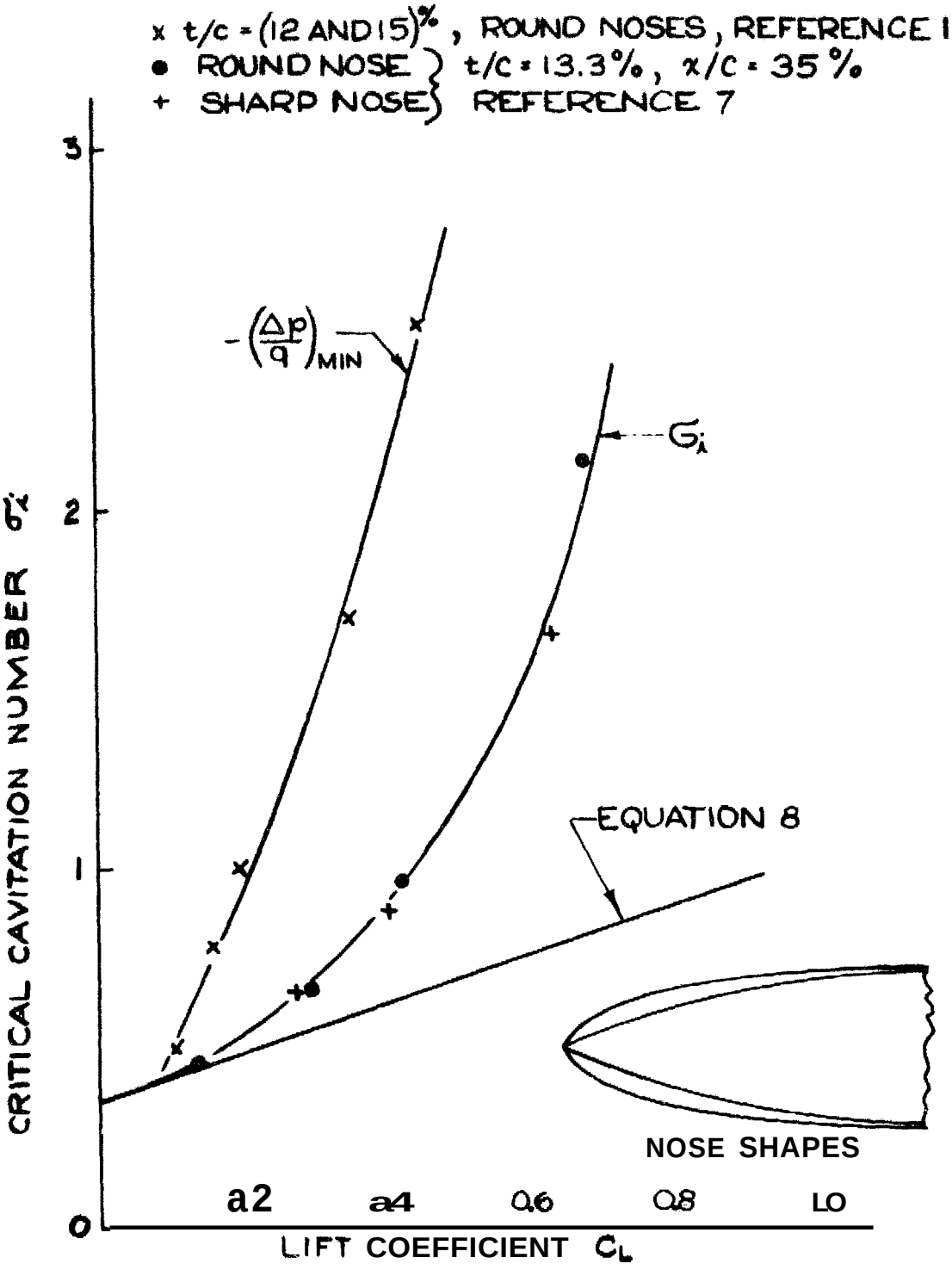

THE CRITICAL CAVITATION NUMBER
OF SYMMETRICAL SECTIONS

GIBBS & COX INC. GRAPH NO. HGR13531-2-SI-1-125 JULY 1952

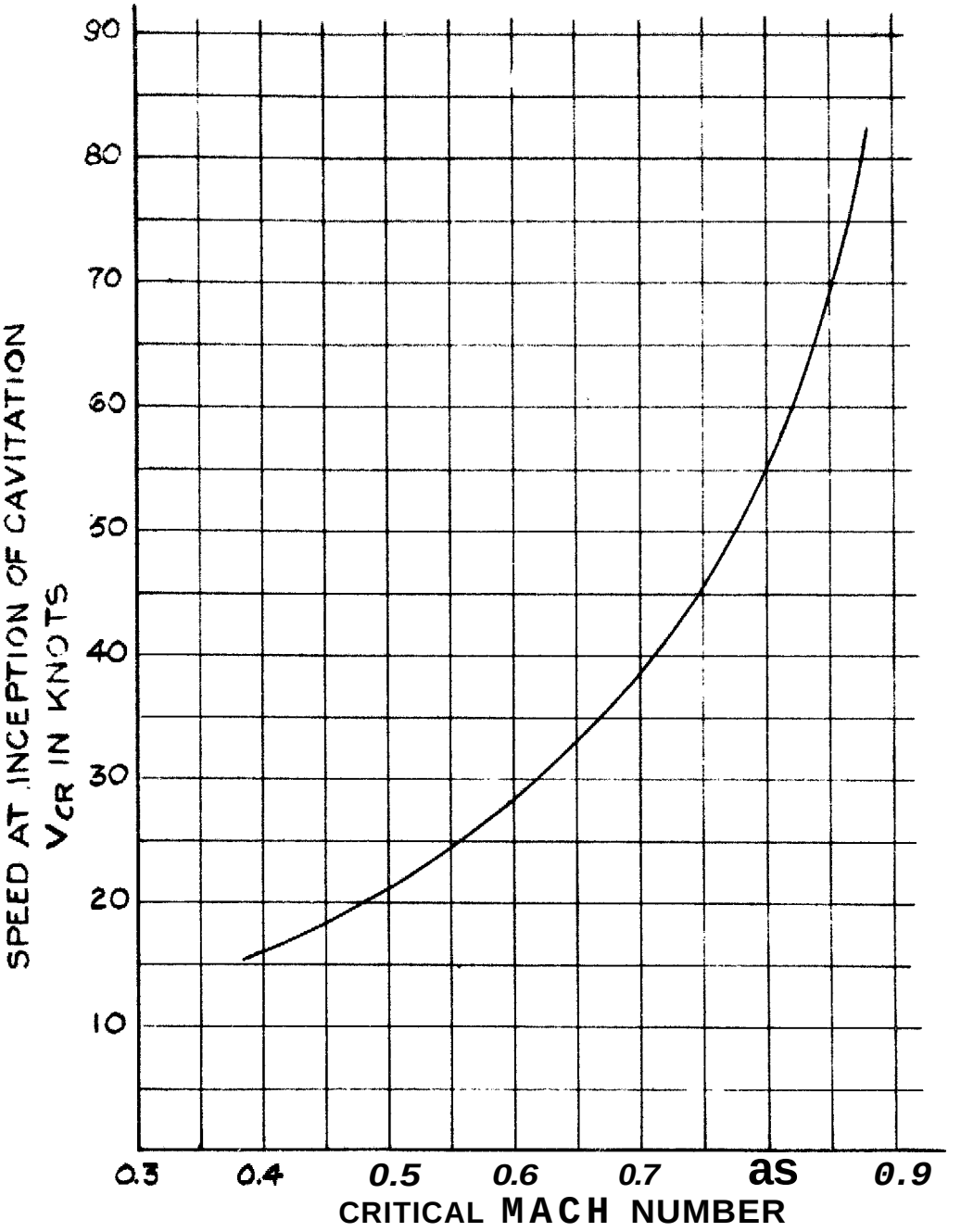

SPEED AT INCEPTION OF CAVITATION AS A FUNCTION OF THE CRITICAL MACH NUMBER

GIBBS & COX INC. GRAPH NO. HGR 13531-2-SI-1-133 AUGUST 1952

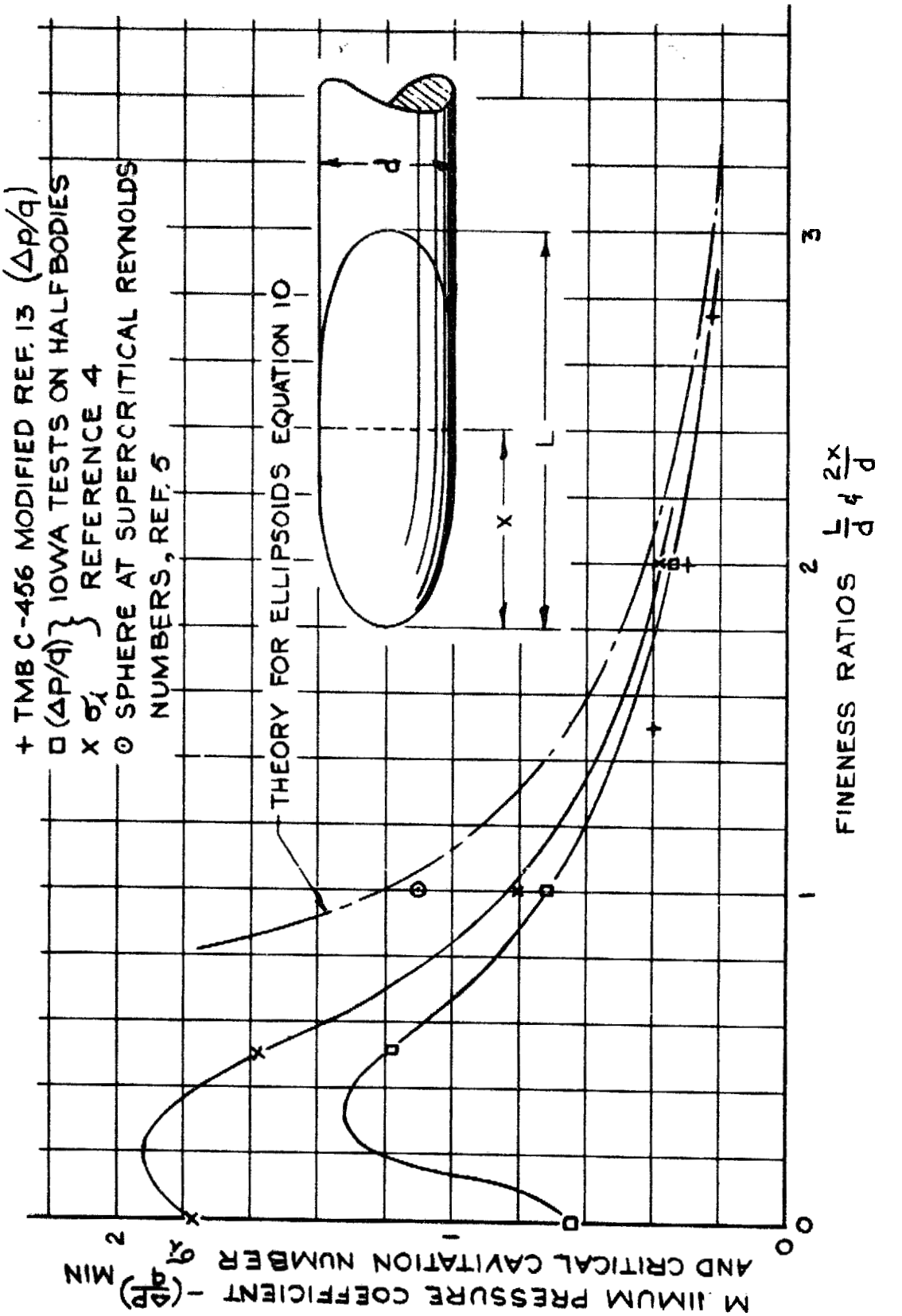

CRITICAL CAVITATION NUMBERS OF THREE-DIMENSIONAL BODIES

GIBBS & COX INC. GRAPH NO. HGR 13531-2-SI-1-134 AUGUST 1952

FIGURE NO. 10

CONFIDENTIAL

STANDARDIZED RELATION OF SPEED & CRITICAL CAVITATION NUMBER

GIBBS & COX INC. GRAPH NO. HGR 13531-2-SI-1-132 AUGUST 1952

FIGURE NO. 11

CONFIDENTIAL

GIBBS & COX, INC.

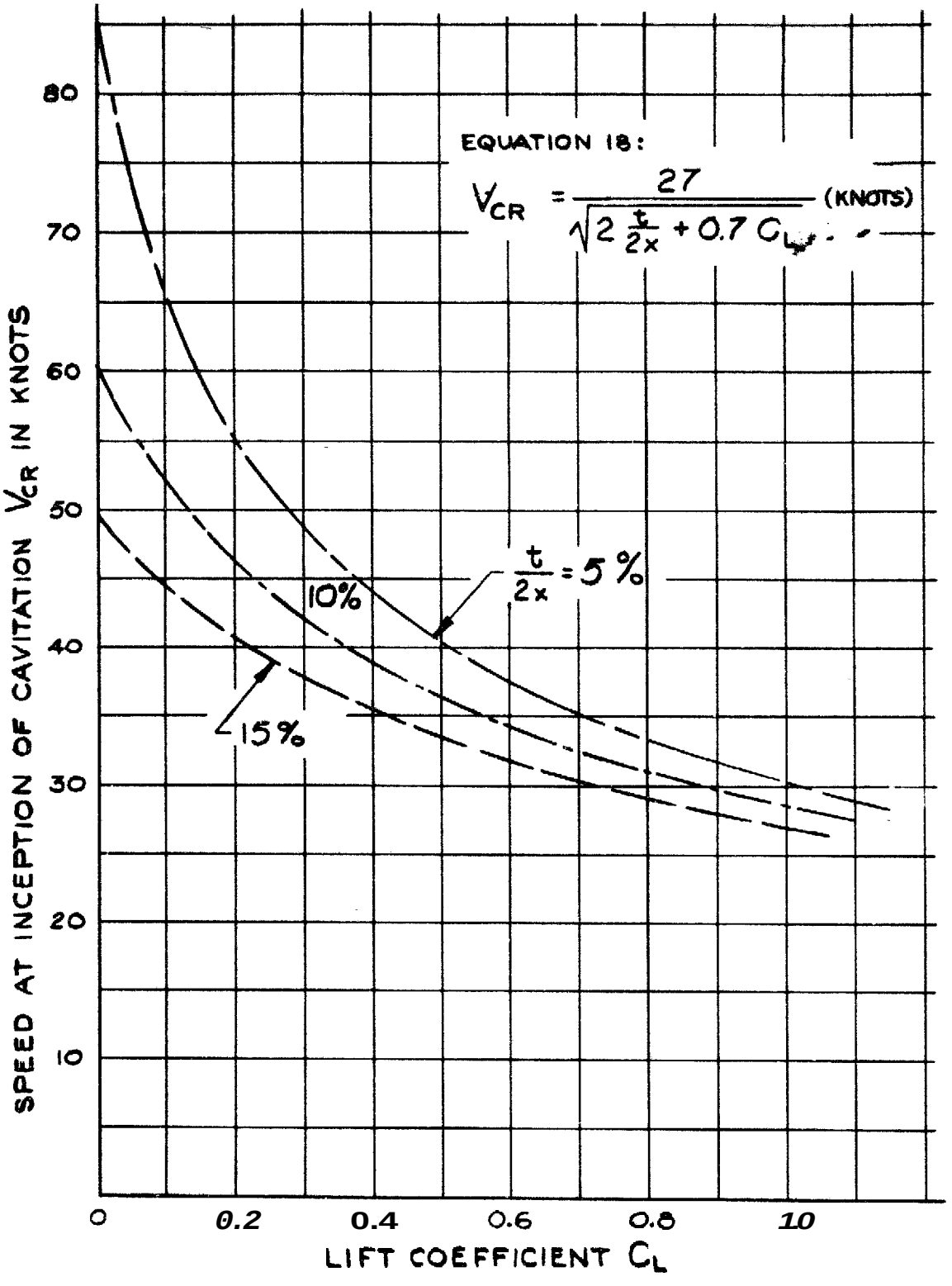

CRITICAL CAVITATION SPEED OF HYDROFOILS

GIBBS & COX INC. GRAPH NO. HGR 13531-2-SI-1-131 AUGUST 1952